Wille, Marie-Luise, Almualimi, Majdi A., & Langton, Christian M.
(2016)
Pulse-echo ultrasound transit time spectroscopy: A comparison of experimental measurements and simulation prediction.
Proceedings of the Institution of Mechanical Engineers, Part H: Journal of Engineering in Medicine, *230*(1), pp. 20-29.

https://doi.org/10.1177/0954411915615911

Pulse-echo ultrasound transit time spectroscopy; a comparison of experimental measurement and simulation prediction

Marie-Luise Wille[1], Majdi A. Almualimi[1] and Christian M. Langton[1]

[1] Institute of Health and Biomedical Innovation, Queensland University of Technology, Australia

Corresponding author:

Marie-Luise Wille, Institute of Health and Biomedical Innovation, Queensland University of Technology, 60 Musk Avenue, Kelvin Grove, QLD 4059, Australia.

Email: m.wille@qut.edu.au

Abstract

Considering ultrasound propagation through complex composite media as an array of parallel sonic rays, a comparison of computer simulated prediction with experimental data has previously been reported for transmission mode (where one transducer serves as transmitter, the other as receiver) in a series of ten acrylic step-wedge samples, immersed in water, exhibiting varying degrees of transit time inhomogeneity. In this study, the same samples were used but in pulse-echo mode, where the same ultrasound transducer served as both transmitter and receiver, detecting both 'primary' (internal sample interface) and

'secondary' (external sample interface) echoes. A transit time spectrum (TTS) was derived, describing the proportion of sonic rays with a particular transit time.

A computer simulation was performed to predict the transit time and amplitude of various echoes created, and compared with experimental data. Applying an amplitude-tolerance analysis, 91.7±3.7% of the simulated data was within ±1 standard deviation (STD) of the experimentally measured amplitude-time data.

Correlation of predicted and experimental transit time spectra provided coefficients of determination (R^2) ranging from 100.0% to 96.8% for the various samples tested.

The results acquired from this study provide good evidence for the concept of parallel sonic rays. Further, deconvolution of experimental input and output signals has been shown to provide an effective method to identify echoes otherwise lost due to phase cancellation. Potential applications of pulse-echo ultrasound transit time spectroscopy (PE-UTTS) include improvement of ultrasound image fidelity by improving spatial resolution and reducing phase interference artefacts.

Keywords: Ultrasound pulse-echo, transit time spectrum, phase interference, ultrasound propagation.

1. Introduction

Conventional piezoelectric ultrasound transducers are phase-sensitive; for two received waves, the degree of phase interference ranges from constructive (in-phase, sum of amplitudes) to destructive (out-of-phase, subtraction of amplitudes).

Many studies have investigated the influence of ultrasound phase interference since the 1950's. The effects of diffraction on attenuation measurements using a matched-pair of quartz transducers was described in 1956 by Seki, Granato, and Truell (2). In 1963, Truell and Oates published a short paper describing phase cancellation effects on velocity and attenuation measurements from samples with non-parallel sides (3). Petley et al. (4) demonstrated that the effect of phase cancellation may be minimised by reducing the size of the receive aperture. Cheng et al. (5) suggested that it is possible to capture most of the propagating ultrasound wave when using a receiver aperture size that corresponds to the size of the transmitting transducer in a confocal set-up.

Bauer et al. (6-9) addressed the dependence of measurement accuracy upon the relative dimensions of the receive aperture.

For an ultrasound wave having propagated through a test sample, the receive-transducer output signal corresponds to the sum of all individual signals detected within its spatial aperture.

Langton has proposed that phase interference effects may be the primary attenuation mechanism associated with ultrasound propagation through complex porous solid:liquid composite media such as cancellous bone, created by inhomogeity in propagation transit time over the phase-sensitive surface of the receiving ultrasound transducer (10). Langton has further suggested that ultrasound propagation through such media may be considered as an array of parallel ‘sonic rays’, the transit time of each being determined by the proportion of two components; being a minimum (t_{min}) when solely through (higher velocity) solid, and a maximum (t_{max}) when solely through (lower velocity) liquid. It should be noted that phase interference would not occur if the velocity of the two materials was equal. A Transit Time Spectrum (TTS) may be derived via deconvolution of the experimentally measured input and output ultrasound signals, thereby describing the proportion of sonic rays having a particular transit time (t_i) (11). Langton and Wille have recently validated this concept in transmission mode, comparing experimental measurements with computer simulation predictions of ultrasound propagation in a range of simplistic solid:liquid step-wedge models exhibiting an extensive variability of transit time inhomogneity (12). In transmission mode, where one ultrasound transducer serves as transmitter and the other as receiver, the detected ultrasound signal consists primarily of 'forward' transmission sonic rays; noting that a double-reflection within a material layer will create a secondary forward sonic ray.

The aim of this study was to validate the sonic ray concept, but in pulse-echo mode; where the same ultrasound transducer serves as both transmitter and receiver; detecting both 'primary' (internal sample interface) and 'secondary' (external sample interface) echoes.

2. Methods

2.1 Samples

Ten acrylic cylindrical shaped step-wedge samples of 20 mm overall depth and 25.1 mm diameter (equal to the ultrasound transducer outer diameter) and exhibiting varying degrees of transit time inhomogeneity were studied. A photograph of the samples is shown in Figure 1 (model ‘b’ to ‘k’) and summarised in Table 1.

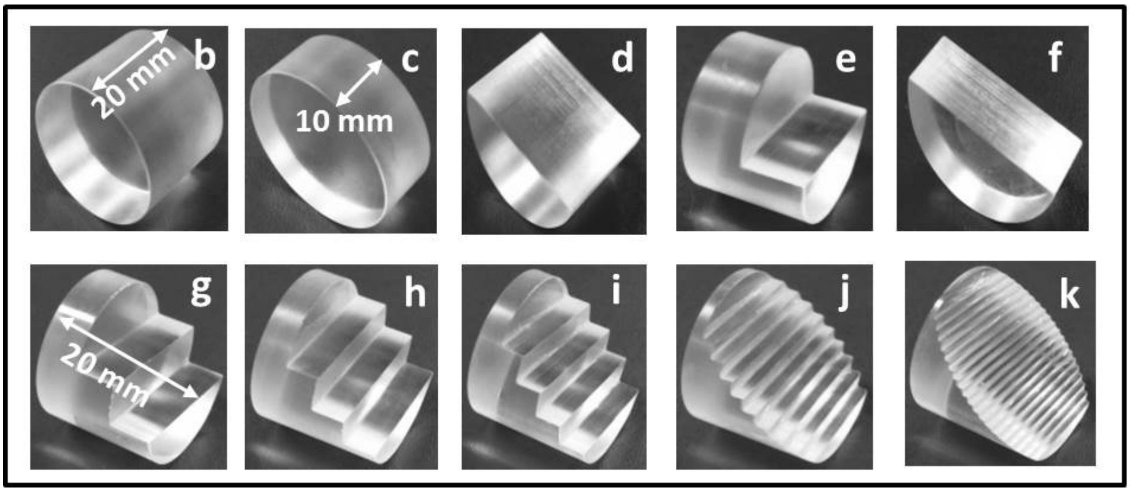

Figure 1. Photograph of models used. Model (a), solely water, served as a reference and is not shown in this figure.

Table 1. Summary of the models used.

Model	Description
a	Water (reference)
b	Solid acrylic cylinder
c	Acrylic cylinder of half-depth, i.e. 50% acrylic, 50% water, normal interface to ultrasound propagation
d	Acrylic half cylinder, i.e. 50% acrylic, 50% water, parallel interface to ultrasound propagation
e	Structure of 75% acrylic and 25% water
f	Structure of 75% water and 25% acrylic
g	Wedge structure, 3 steps
h	Wedge structure, 4 steps
i	Wedge structure, 5 steps
j	Wedge structure, 10 steps
k	Wedge structure, 20 steps

2.2 Experimental setup

A single element, unfocused, ¾'' diameter, 1 MHz broadband ultrasound transducer (Harisonics I7-0112-G, Olympus NDT, Waltham, MA, USA) was connected to a pulser-receiver unit (Model 5800PR, Panametrics, Waltham, MA, USA), operating with a 400V voltage spike. The -6 dB bandwidth of the transducer was 0.63 MHz with a centre frequency of 0.8 MHz and the pulse length 3.1 μs. The receiver output was connected to a 14-bit digitiser card

(National Instruments PCI5122, Austin, TX, USA) operating at 50 MHz digitisation rate; 5000 data points were collected corresponding to a recording time of 100 μs. The transducer and sample were placed coaxially in a water bath, with a highly acoustically-reflective flat-normal interface positioned at the opposite side of the sample (Figure 2), thereby creating an echo at the far-side of a sample. The distance between the transducer and the reflective interface was 65 mm and the maximum height of each sample was 20 mm.

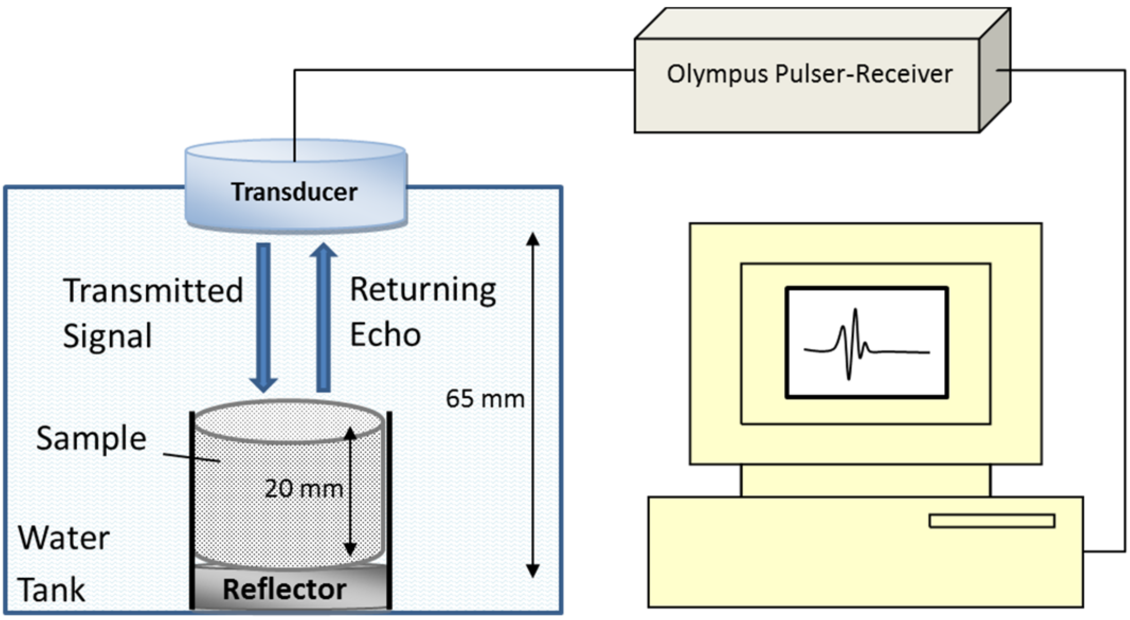

Figure 2. Schematic diagram illustrating the experimental set-up; model 'b', 100% acrylic, is indicated in this sketch. The transducer-reflector separation was 65 mm.

2.3 Computer simulation

The computer simulation was performed using MATLAB (The MathWorks Inc., Natick, MA, USA) to replicate the ultrasound signal detected by the ultrasound transducer; being a mathematical convolution of the transit time spectrum and the input ultrasound signal. The input (reference) ultrasound signal for the computer simulation was experimentally derived by recording the ultrasound echo signal through water alone (model 'a').

The term 'primary echo (E_p)' was utilised to describe those emanating from the 'front face' of each step-wedge element; 'secondary echoes (E_s)' describe those emanating from the 'back wall' of each step-wedge element, as shown in Figure 3 for models 'a' to 'f'.

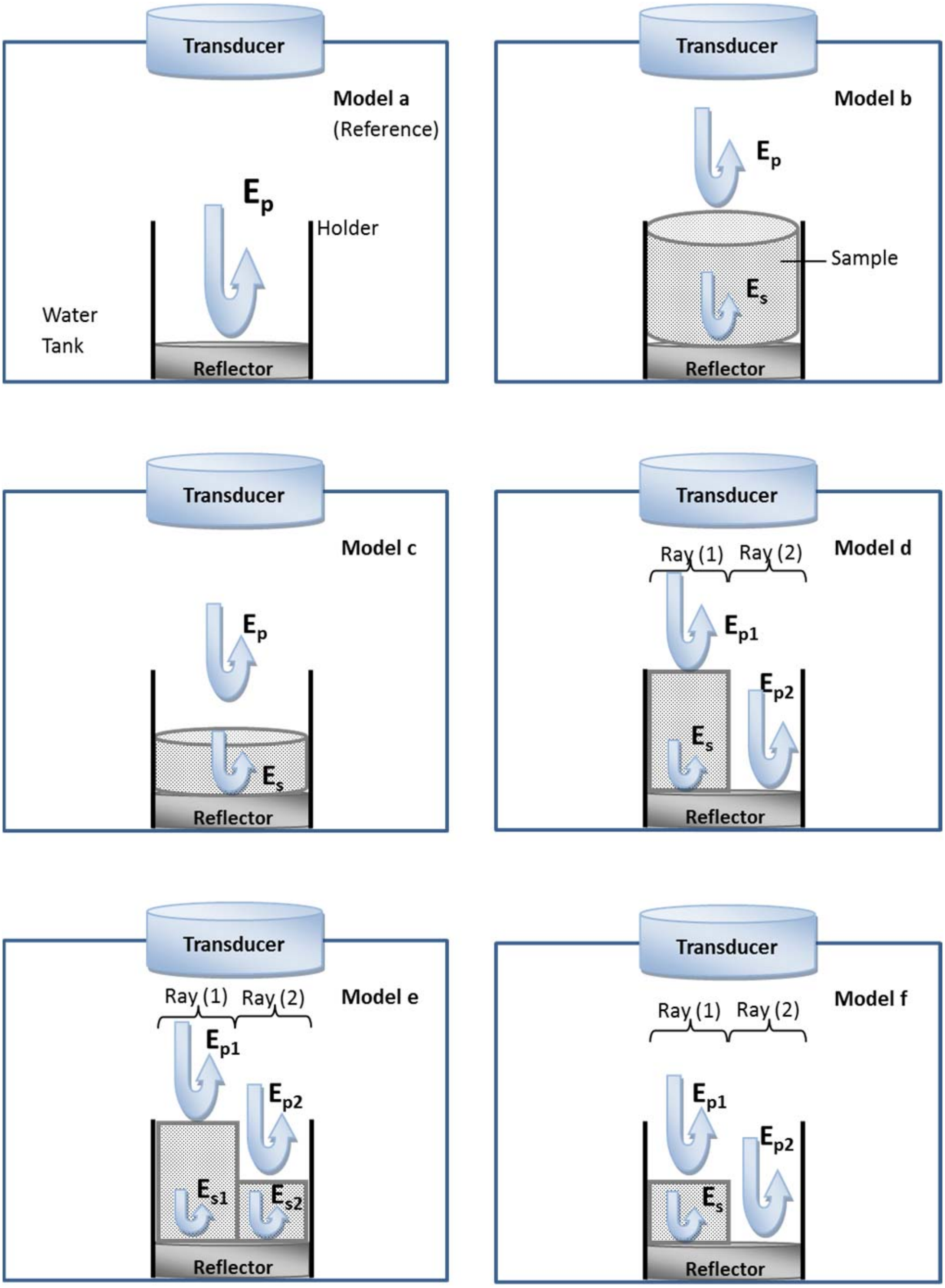
Transducer
Model a
(Reference)
Ep
Holder
Water
Tank
Reflector
Transducer
Model b
Ep
Sample
Es
Reflector
Transducer
Model c
Ep
Es
Reflector
Transducer
Model d
Ray (1)
Ray (2)
Ep1
Ep2
Es
Reflector
Transducer
Ray (1)
Ray (2)
Model e
Ep1
Ep2
Es1
Es2
Reflector
Transducer
Model f
Ray (1)
Ray (2)
Ep1
Ep2
Es
Reflector

1

Figure 3. Schematic diagram describing the creation of primary (E_p) and secondary (E_s) echoes for models ‘a’ to ‘f’. Model ‘a’ is water only, and serves as a reference signal.

The transit time (t) corresponding to each primary and secondary echo, for each sample and step-wedge element, was calculated using Equation 1,

$$t = \frac{2d_a}{v_a} + \frac{2d_w}{v_w} \quad (1)$$

where d_a and d_w are the sample dimensions of acrylic and water; v_a and v_w are the ultrasound velocities in acrylic (2680 ms^{-1}) and water (1493 ms^{-1}) both measured experimentally at a temperature of 23.6 °C. The simulated ultrasound signal is a combination of all primary and secondary echoes for a given sample.

The amplitude of each primary or secondary echo, from each sample and step-wedge element, was calculated based upon i) the relative area of the step-wedge element (hence corresponding to the relative transducer reception area), ii) the attenuation coefficient in acrylic (assuming the attenuation in water to be zero), and iii) the amplitude reflection coefficient of the corresponding echo-forming interface.

2.3.1 Relative step-wedge element and transducer-reception area

Since the samples and transducer face are circular in cross-section, a step-wedge element (and corresponding transducer reception) area (A), being orthogonal to both the ultrasound propagation direction and the continuous plane of the step-wedge element, has a maximum value at the centre of the sample and a minimal value at the perimeter. This segment area may be calculated using Equation 2

$$A = \frac{r^2(\theta - sin\theta)}{2} \quad (2)$$

where r is the radius of the sample and θ is the angle subtended between a segment of height h from the perimeter and the chord, as sketched in Figure 4, given by

$$\theta = 2 \cdot arcos(\frac{r-h}{r}) \quad (3)$$

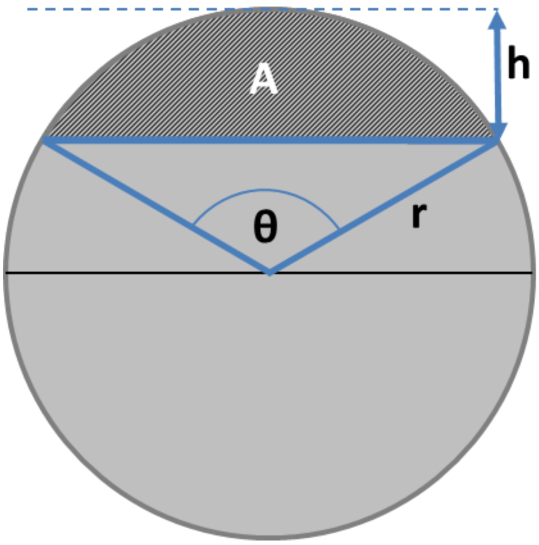

Figure 4. Calculation of segment area A; where r is the radius of the sample and θ is the angle subtended between a segment of height h from the perimeter and the chord.

For a step ranging from heights h_1 to h_2, the area of the wedge step is obtained by subtracting the two corresponding segment areas.

2.3.2 Attenuation coefficient

The attenuation coefficient of acrylic at a frequency of 1 MHz is 25.3 Np m^{-1} (based upon 57 Npm^{-1} quoted at 2.25 MHz for Perspex, being similar to acrylic (13) and assuming a linear relationship between attenuation coefficient and frequency). The attenuation coefficient is in agreement with experimental measurement of sample models (b) and (c), being 25.5 ± 0.05 Np m^{-1}.

2.3.3 Reflection and transmission amplitude coefficients

Consider an ultrasound wave propagating through a material of density ρ_1 (kg m^{-3}) at a velocity of v_1 (m s^{-1}), normally incident upon a flat perpendicular interface with a material of density ρ_2 (kg m^{-3}) and propagation velocity v_2 (m s^{-1}). The corresponding acoustic impedances (Z_1, Z_2) for the two materials are defined as the product of their respective density and velocity ($\rho \cdot v$), being $3.16 \cdot 10^6$ kg m^{-2} s^{-1} for acrylic and $1.49 \cdot 10^6$ kg m^{-2} s^{-1} for water. The amplitude reflection (RC) and transmission (TC) coefficients at the interface are defined in Equation 3 and 4. No echo is created when Z_1=Z_2 (TC = 1 and RC = 0); if Z_1>Z_2 (RC is negative, acrylic into water), the reflected wave is phase-inverted; and if Z_1<Z_2 (RC is positive, water into acrylic) the amplitude of the transmitted wave is higher than that of the incident wave.

Reflection Coefficient $$RC = \frac{Z_2 - Z_1}{Z_2 + Z_1} \quad (3)$$

Transmission Coefficient $$TC = \frac{2Z_2}{Z_2 + Z_1} \quad (4)$$

2.3.4 Detected ultrasound signal

The predicted overall amplitude of each primary or secondary echo for a given sample and step-wedge element, as received by the ultrasound transducer, was calculated as the product of the attenuation coefficient, the relative step-wedge element area, and the corresponding interface reflection coefficient.

The ultrasound signal detected by the ultrasound transducer for each sample was simulated by convoluting the input ultrasound signal with the corresponding Transit Time Spectrum; being a combination of all primary and secondary echoes, noting the overall amplitude and transit time of each echo.

We can now describe the simulated output signal with following equation:

$$\text{Simulated o/p} = (\text{experimental i/p} \cdot \mu \cdot A \cdot RC \cdot TC) * TTS \qquad (5)$$

Where o/p and i/p denotes output and input signal, μ is the attenuation coefficient; A is the relative segment area, RC and TC the reflection and transmission coefficient, and TTS the transit time spectrum. Here * describes the convolution operator.

3. Results and discussion

This study examined the feasibility of applying the ultrasound transit time spectroscopy concept in pulse-echo mode. The experimental and computer simulation approaches were fundamentally similar to those previously reported for transmission mode [12]. The differences for pulse-echo were a) the same ultrasound transducer is used for both transmission and reception, and b) the computer simulated prediction of the transit time spectrum considered a combination of internal (primary) and external (secondary) sample interface echoes rather than through-sample transmission.

Even though the experimental output signals were subject to significant phase cancellation, the deconvolution technique was able to unfold the signal and identify the primary and secondary echoes.

The expected number of primary and secondary echoes for each model is shown in Table 2. The received ultrasound signals for experimental measurement (red-dashed) and simulation prediction (blue-solid) for each sample, in both time- and frequency-domain, are shown in Figure 5; demonstrating good agreement between the two approaches.

The time-domain agreement between experimental and simulated is higher, as to be expected, in cases where discrete signals are present (models 'a'-'f'); the level of agreement decreasing with increasing complexity of the sample and corresponding transit time spectrum. By definition, the computer simulation predicted transit time spectrum only contains primary and secondary echo components; it does not consider echoes emanating from 'double-reflections' within a layer. Such 'tertiary echoes' may however exist within the experimental data, for example, emanating from a short-depth acrylic step-wedge element. These tertiary echoes also have the potential to create phase interference with primary and secondary echoes; thereby modifying the format of the received ultrasound signal.

The frequency-domain plots show good qualitative agreement between the experimental and simulated signals, as demonstrated by the spectral detail. Further, the frequency profiles indicate constructive and destructive interference behaviour which matches the time domain observation. It should also be noted that the frequency plots also demonstrates the bandwidth theorem; a short signal in the time-domain has a broad frequency-spectrum (model 'a'), and vice versa (model 'k', 20-step wedge).

Table 2. Number of steps and corresponding sonic rays in each model and the expected primary and secondary echoes.

Model	Number of steps	Number of rays	Expected number of		Total number of echoes
			Primary echoes	Secondary echoes	
a	0	1	1	0	1
b	1	1	1	1	2
c	1	1	1	1	2
d	1	2	2	1	3
e	2	2	2	2	4
f	1	2	2	1	3
g	3	3	3	3	6
h	4	4	8	4	8
i	5	5	5	5	10
j	10	10	10	10	20
k	20	20	20	20	40

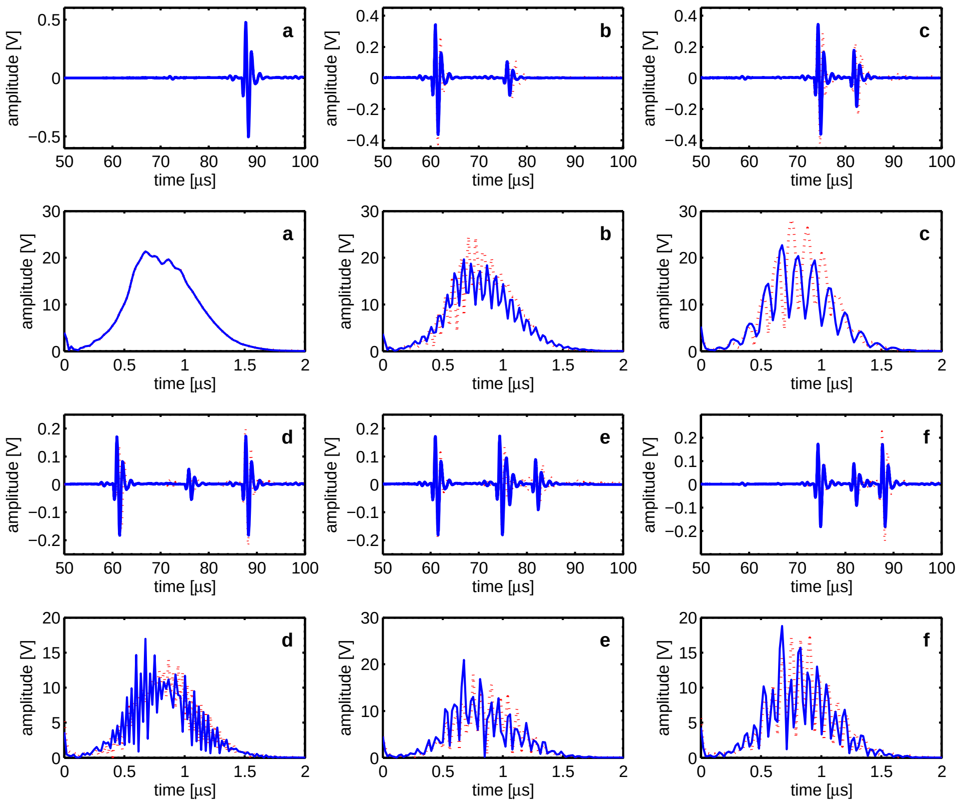
a
b
c
d
e
f
amplitude [V]
time [µs]

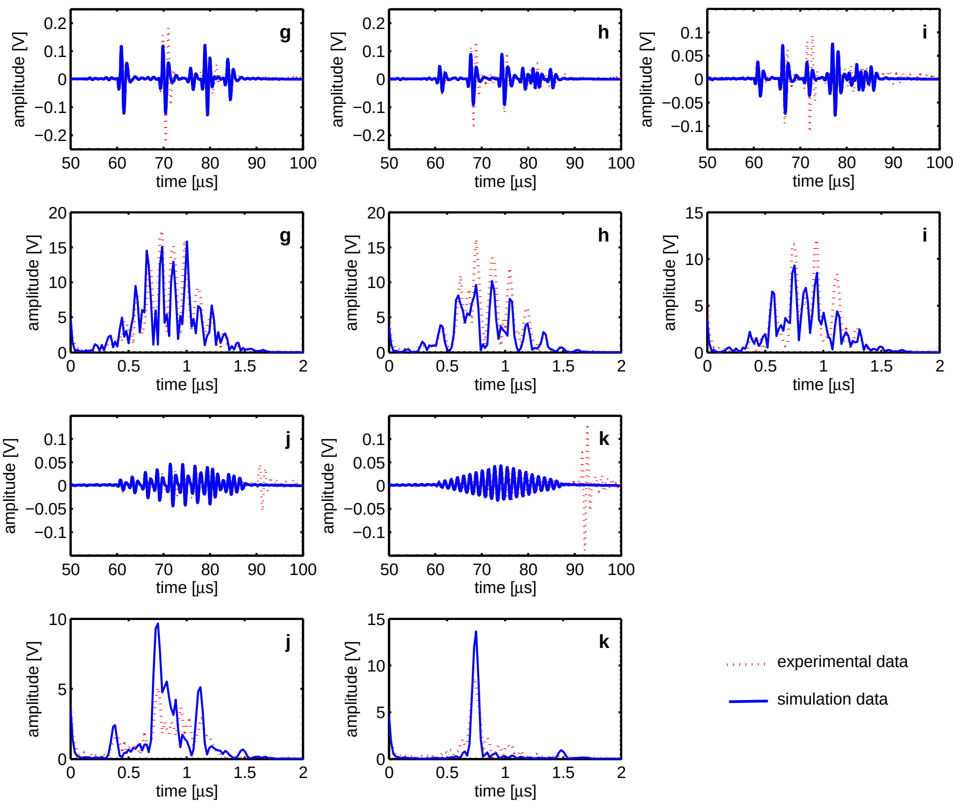

The signals corresponding to the models ’b’ and ‘c’ (no step, single acrylic/water interface normal to propagation) consist of single primary and secondary echoes; a decrease in acrylic thickness resulted in an increase in amplitude (due to signal attenuation in acrylic) and shorter time spacing between primary and secondary echoes. The received signal of model ‘d’ (acrylic and water compartments were parallel to ultrasound propagation) resulted in two primary echoes from water/acrylic and acrylic/reflector respectively; plus a single acrylic/water secondary echo, as shown in Figure 3 (model 'd').

Table 3. Comparison of the calculated time of flight (TOF) with experimental measurements for discrete signals. E denotes 'echo', with the subscripts 'P', 'S', and 'T' being primary, secondary, and tertiary echoes.

Model	Ray Type	Path Length (mm)		Calculated TOF (µs)	Experimental TOF (µs)	% of agreement
		Water	Acrylic			
a	E_p	65.0	-	87.1	87.1	100.00
b	E_p	44.0	-	60.3	60.5	99.65
	E_s	44.0	20.0	75.2	77.2	97.35
c	E_p	54.5	-	73.7	71.7	97.3
	E_s	54.5	10.0	81.2	84.6	95.75
d	E_{p1}	44.0	-	60.3	63.2	95.17
	E_s	44.0	20.0	75.2	77.5	96.96
	E_{p2}	65.0	-	87.1	88.1	98.83
e	E_{p1}	44.0	-	60.3	60.3	99.98
	E_{p2}	54.5	-	73.7	72.4	98.25
	E_{s2}	54.5	10.0	81.2	82.6	98.21
f	E_{p1}	54.5	-	73.7	75.3	97.79
	E_s	54.5	10.0	81.1	83.1	97.57
	E_{p2}	65.0	-	87.1	86.2	99.00
g	E_{p1}	44.0	-	60.3	60.3	99.95
	E_{s1}	44.0	20.0	75.2	76.8	97.86
	E_{p2}	51.7	-	69.2	69.2	99.94
	E_{s3}	58.4	6.6	83.2	85.7	96.96
h	E_{p1}	44.0	-	60.3	60.3	99.95

	E_{p2}	50.0	-	67.0	67.0	99.94
	E_{p3}	54.5	-	73.7	73.7	99.96
i	E_{p1}	44.0	-	60.2	60.2	99.93
	E_{p2}	49.0	-	65.6	65.5	99.85
	E_{p3}	52.9	-	70.8	70.8	99.97
j	E_T	62.9	2.1	93.7	93.0	99.25
k	E_T	63.9	1.1	93.9	93.0	99.08
Mean (% of agreement)						98.63
Standard deviation (% of agreement)						1.43

When the transit time difference between any combination of echoes, primary and/or secondary, is less than the ultrasound pulse length, phase interference will occur. The step-wedge elements were equal in height and depth; hence, as the number of elements increased, the depth of each element reduced, thereby reducing the transit time difference between adjacent elements. The degree of phase interference increases with an increasing number of overlapping echoes, being a maximum for model 'k' with 20-step-wedges, where near total destructive interference is evident.

An additional experimental signal echo at approximately 93 μsec was observed for models 'j' and 'k'; it is considered that this echo corresponds to a 'tertiary' multiple-echo within the first (minimum acrylic thickness) step of each model (Table 3). The amplitude of this signal is higher in model 'k' compared to model 'j' due to the lower thickness of acrylic propagated and hence lower absorption.

In order to quantitatively determine the agreement between experimental and computer simulation approaches, a threshold-based analysis was developed and implemented. The standard deviation (STD) of experimental ultrasound signal amplitude was calculated for each sample. From this, amplitude-tolerance bands of ±0.5, ±1 and ±1.5 standard deviations (STD) were applied to the experimentally measured signal trace amplitude for each corresponding sample. The proportion of computer simulation predicted ultrasound signal data points within each amplitude-tolerance band was then calculated.

Each experimental measurement was repeated four times, the coefficient of variation for amplitude (CV% = STD/Mean) being less than 0.8%, demonstrating negligible variation. The proportion of simulation data points within each amplitude tolerance band, for each model, is illustrated in Figure 7. As expected, the proportion increased with broader tolerance band; when averaged over all samples, the proportions were 75.3±12.9%, 86.2±7.4% and 91.7±3.7% for ±0.5STD, ±1 STD, and ±1.5 STD thresholds respectively.

[insert Figure 6.]

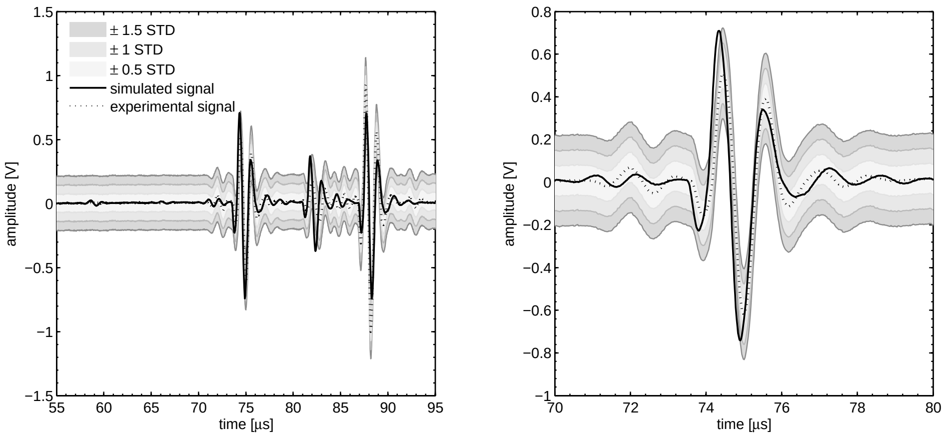

Figure 6. Threshold-based analysis of the experimental and simulated output signals for model ‘f’ (25% acrylic, 75% water). Comparison of experimentally measured (dotted line) and simulated (solid line) output signals, amplitude tolerance bands of ±0.5STD (light grey), ±1 STD (middle grey), and ±1.5 STD (dark grey) were applied to the experimental data and the proportion of simulation data points within the tolerance bands determined. The plot on the right hand side provides a magnified view of the initial echo for improved visualisation; the legend entries are the same.

[insert Figure 7.]

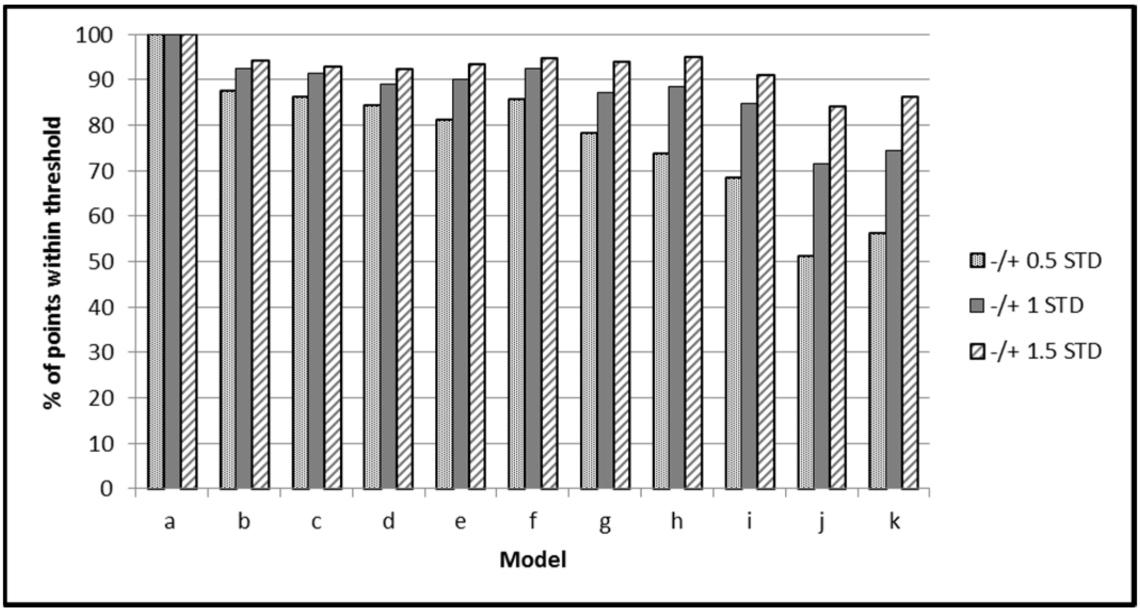

Figure 7. Results of the threshold-based analysis of the experimental and simulated output signals: the 3 bars for each model correspond to the 3 applied tolerance bands of ±0.5 STD (dotted), ±1 STD (solid grey), and ±1.5 STD (striped) of the experimental amplitude.

Further quantitative comparative analysis of computer-simulation predicted and experimental approaches was performed by comparing the temporal position of spectral peaks within the corresponding transit time spectra. To remove spectral-peak noise artefacts from each deconvolution-derived experimental transit time spectra, a cut-off threshold of 10% of maximum spectral peak amplitude was applied. Transit time agreement between predicted and experimental data was then determined using the nearest point search *dsearchn* function within Matlab; for two vectors x (experimental data) and y (simulation data), *k*=desearchn(x, y) returns the indices *k* of the closest point in x for each point in y. This was used instead of a standard correlation comparison since the resulting experimental and predicted transit time vectors were not necessarily of the same lengths, therefore only matched spectral components were considered. Figure 8 shows the experimental (dashed grey bar) and simulation (solid black line) transit time spectra for model 'h' and 'k' (4- and 20-step-wedge), along with the corresponding regression fit. It is noted that additional echoes were present in the experimental spectra that were not predicted by the computer simulation, as indicated by the arrows in the top left plot of Figure 8. It is considered that these echoes are due to 'tertiary' multiple-echoes (E_T) within an acrylic or water layer.

Table 4 summarizes the correlation of experimental and predicted transit times, the coefficients of determination (R^2%) ranging from 100.0% to 96.8% for the various samples tested; the agreement reducing with increasing sample and corresponding transit time spectral complexity.

[insert Figure 8.]

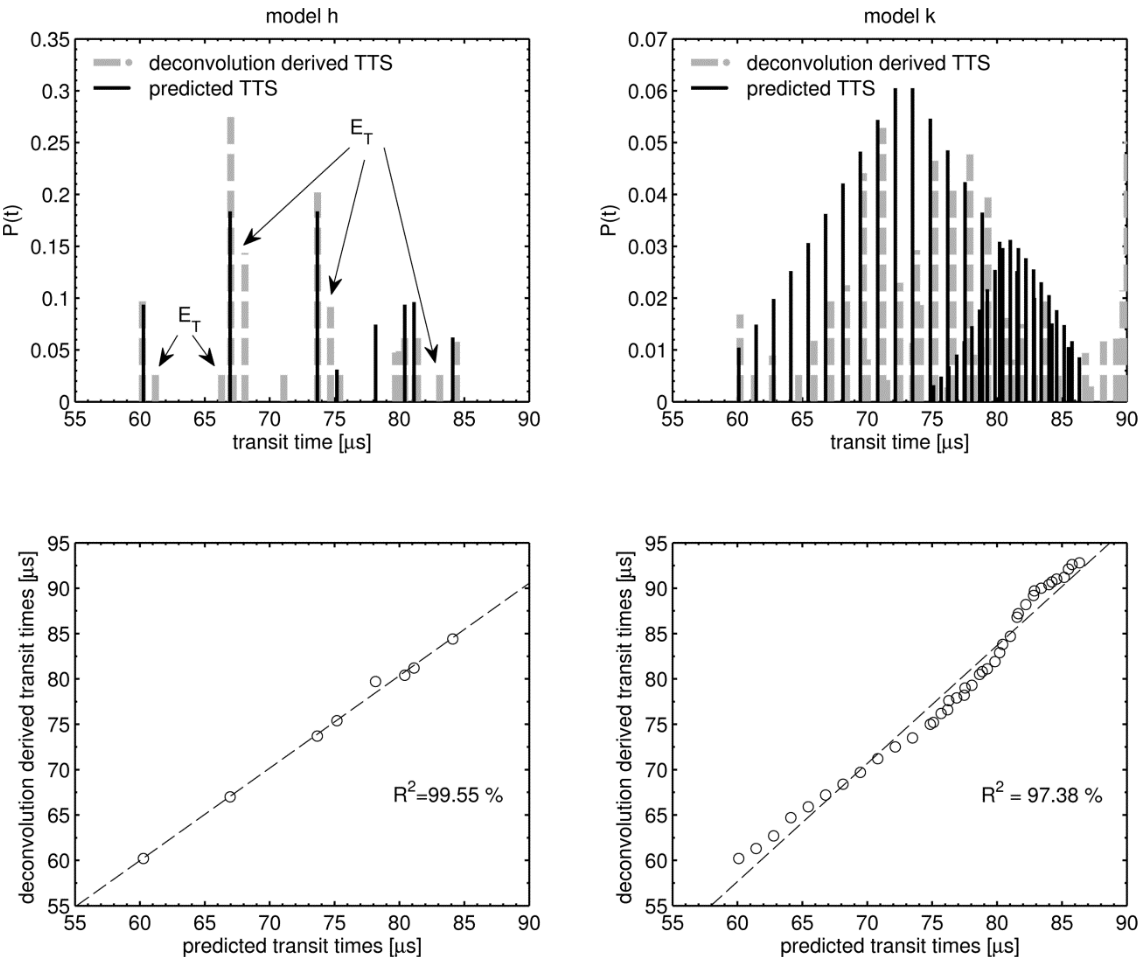

Figure 8. Comparison of the transit time spectra (top row) along with transit time correlation (bottom row) between experimental and predicted data for models 'h' (4 wedge-steps, left column) and 'k' (20 wedge-steps, right column). Tertiary echoes (E_T) are present in the experimental data as indicated by the arrows in the top left plot, but not in the simulation, and were not considered in the linear regression fit.

[insert Table 4.]

Table 4. Coefficient of determination (R^2 in %) of experimentally derived and predicted transit times.

Model	R^2 [%]
a	100
b	99.99
c	99.99
d	99.95
e	99.98
f	99.97
g	98.60
h	99.55
i	99.70
j	96.83
k	97.38

4. Conclusion

The aim of this study was to validate the ‘parallel sonic ray’ concept in ultrasound pulse-echo mode by comparing computer simulation and experimental data. Applying an amplitude-tolerance analysis, an agreement of 91.7±3.7% was observed at a threshold of ±1 STD of the experimental data. Experimental transit times derived via deconvolution were compared to predicted values, the coefficients of determination (R^2%) ranging from 100.0%

to 96.8% for the various samples tested; the agreement reducing with increasing transit time spectral complexity.

The results acquired from this study have provided additional evidence for the concept of parallel sonic rays. Further, deconvolution of experimentally measured input and output signals has been shown to provide an effective method to identify echoes otherwise lost due to phase cancellation. Potential application of pulse-echo ultrasound transit time spectroscopy (PE-UTTS) includes improvement of ultrasound image fidelity by improving special resolution and reducing phase interference artefacts.

Funding

This research received no specific grant from any funding agency in the public, commercial, or not-for-profit sectors.

References

1. Busse L, Miller J. Detection of spatially nonuniform ultrasonic radiation with phase sensitive (piezoelectric) and phase insensitive (acoustoelectric) receivers. The Journal of the Acoustical Society of America. 1981;70:1377.

2. Seki H, Granato A, Truell R. Diffraction effects in the ultrasonic field of a piston source and their importance in the accurate measurement of attenuation. The Journal of the Acoustical Society of America. 1956;28:230.

3. Truell R, Oates W. Effect of lack of parallelism of sample faces on the measurement of ultrasonic attenuation. The Journal of the Acoustical Society of America. 1963;35:1382.

4. Petley G, Robins P, Aindow J. Broadband ultrasonic attenuation: Are current measurement techniques inherently inaccurate? British journal of radiology. 1995;68(815):1212-4.

5. Cheng J, Serra-Hsu F, Tian Y, Lin W, Qin Y-X. Effects of Phase Cancellation and Receiver Aperture Size on Broadband Ultrasonic Attenuation for Trabecular Bone In Vitro. Ultrasound in Medicine & Biology. 2011 12//;37(12):2116-25.

6. Bauer AQ. The role of phase in ultrasonic measurements of phase aberrating media using piezoelectric receivers: Washington University St. Louis; 2009.

7. Bauer AQ, Anderson CC, Holland MR, Miller JG, editors. Measurement artifacts in sonometry of cancellous bone: The relative impact of phase cancellation and interference on measurements of phase-distorting phantoms. Ultrasonics Symposium, 2008 IUS 2008 IEEE; 2008: IEEE.

8. Bauer AQ, Marutyan KR, Holland MR, Miller JG. Is the Kramers-Kronig relationship between ultrasonic attenuation and dispersion maintained in the presence of apparent losses due to phase cancellation? The Journal of the Acoustical Society of America. 2007;122:222.

9. Bauer AQ, Marutyan KR, Holland MR, Miller JG. Negative dispersion in bone: The role of interference in measurements of the apparent phase velocity of two temporally overlapping signals. The Journal of the Acoustical Society of America. 2008;123:2407.

10. Langton CM. The 25th anniversary of BUA for the assessment of osteoporosis: time for a new paradigm? Proceedings of the Institution of Mechanical Engineers, Part H: Journal of Engineering in Medicine. 2011;225(2):113-25.

11. Langton CM, Wille ML, Flegg MB. A deconvolution method for deriving the transit time spectrum for ultrasound propagation through cancellous bone replica models. Proc Inst Mech Eng Part H-J Eng Med. 2014 Apr;228(4):321-9.

12. Langton CM, Wille ML. Experimental and computer simulation validation of ultrasound phase interference created by lateral inhomogeneity of transit time in replica bone: marrow composite models. Proc Inst Mech Eng Part H-J Eng Med. 2013 Aug;227(8):890-5.

13. Kaye GWC and Laby TH. The speed and attenuation of sound. In: Kaye GWC and Laby TH (eds) Tables of physical & chemical constants (online. version 1.1 (2012)).